

**Redefining the chemistry of super-macroporous materials: when dendritic molecules meet
polymer cryogels**

Sergio D. García Schejtman †,‡,§, *Santiago Marzini Irranca* †, *Cecilia I. Alvarez Igarzabal* †,‡ and *Marisa Martinelli* *

†,‡,

† Universidad Nacional de Córdoba. Facultad de Ciencias Químicas. Laboratorio de Materiales Poliméricos (LaMaP).
Córdoba, Argentina.

‡ Instituto de Investigación y Desarrollo en Ingeniería de Procesos y Química Aplicada (IPQA). CONICET. Córdoba,
Argentina.

Supplementary Information

1.1 Synthesis of the dendritic macro-monomer, ABAh

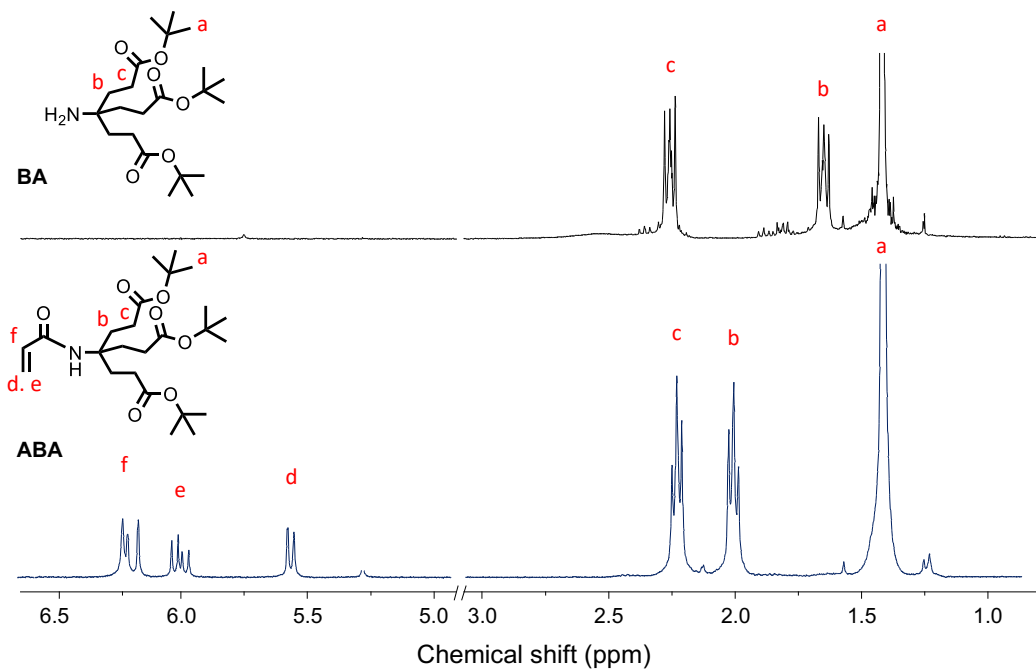


Fig. S1. ¹H-NMR spectra of BA and ABA.

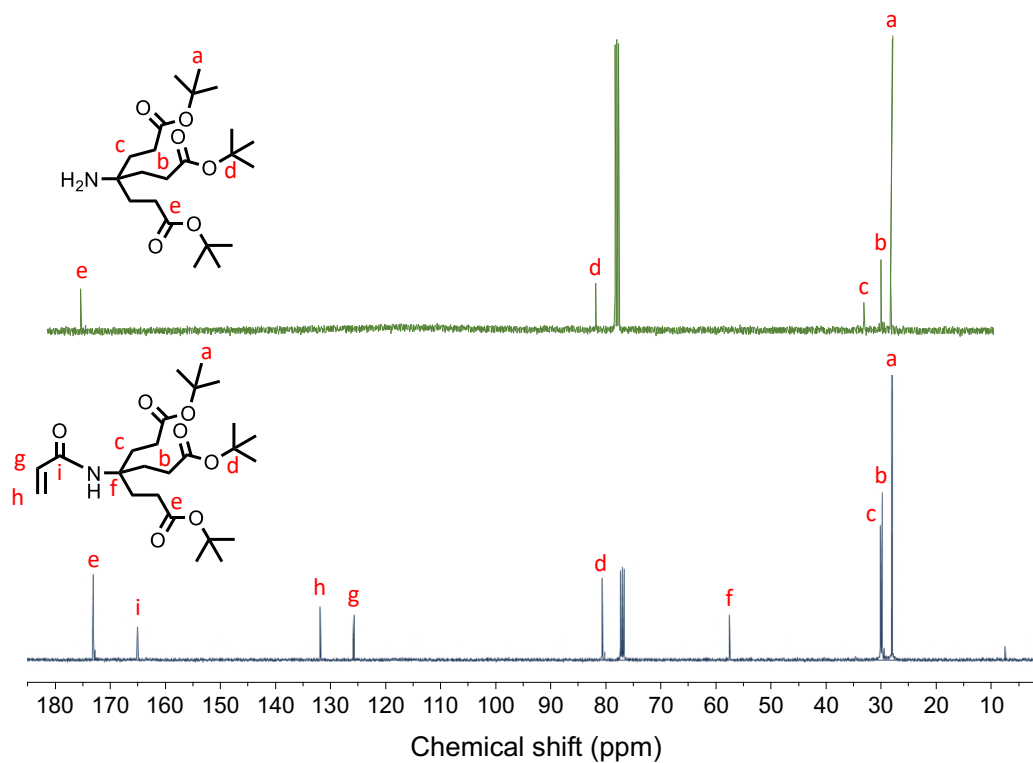


Fig. S2. ¹³C-NMR spectra of BA and ABA.

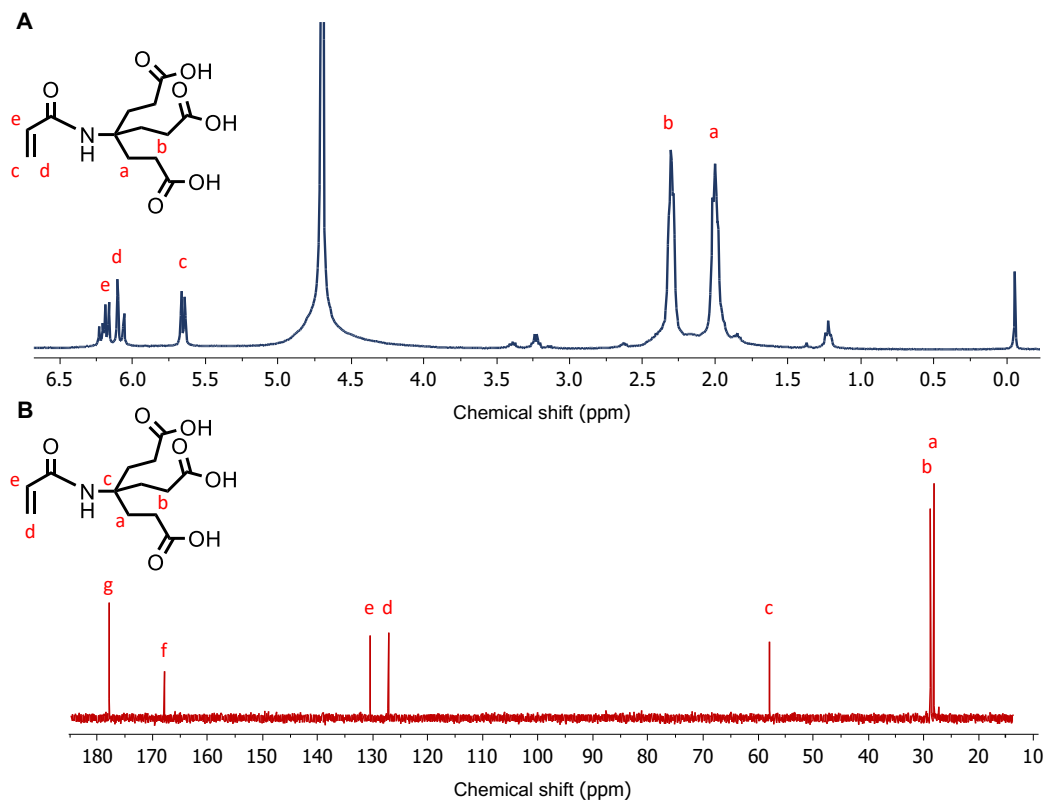


Fig. S3. $^1\text{H-NMR}$ and $^{13}\text{C-NMR}$ spectra of ABAh.

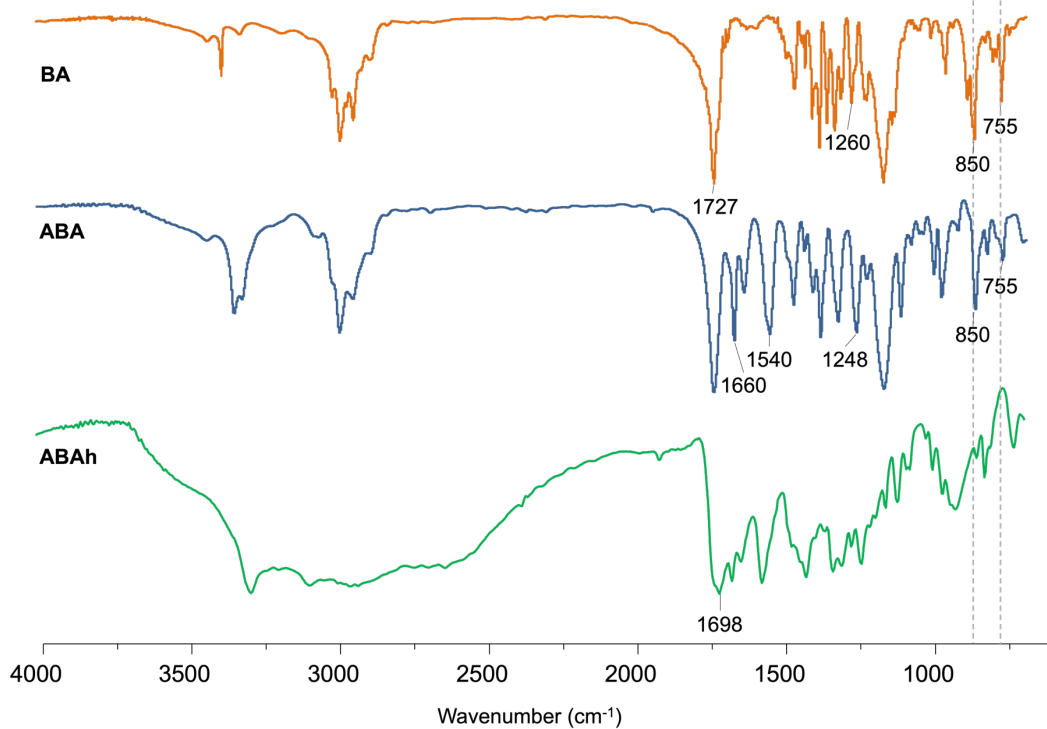


Fig. S4. FT-IR spectra of BA, ABA and ABAh.

1.2 Photo-polymerized dendritic cryogels

The photo-polymerization reaction of the PEG cryogel was followed by RAMAN spectroscopy, as shown in Fig. S5. The first sample (0 min) indicate the reactant mixture before irradiation; in this point, the C=C signal of PEGDMA monomer at 1634 cm^{-1} was observed. When the irradiation time was 10 min, the vinyl signal greatly decreased respect to carbonyl signal (between $1700\text{-}1720\text{ cm}^{-1}$). The monomer conversion to polymer was estimated by the integration of the vinyl and carbonyl signals. Thus, the methodology yielded cryogels with a conversion up to 90% at after 40 min.

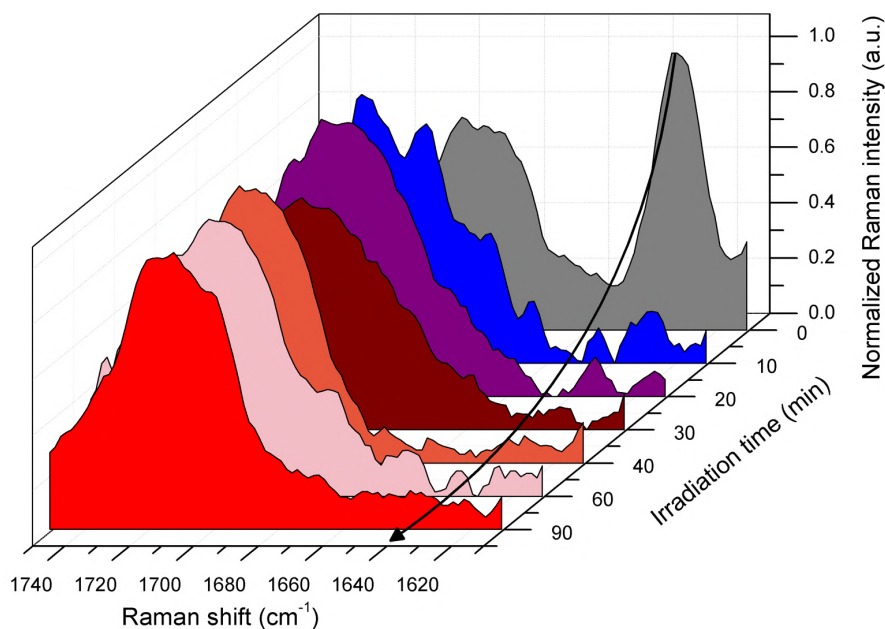


Fig. S5. RAMAN spectra of PEGDMA at different reaction times.

1.3 Optimized mass concentration of PEGDMA in the CGs

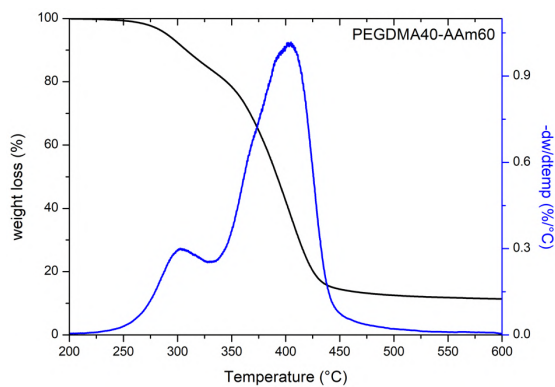
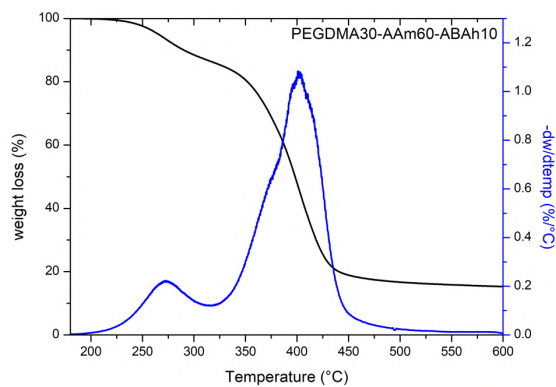
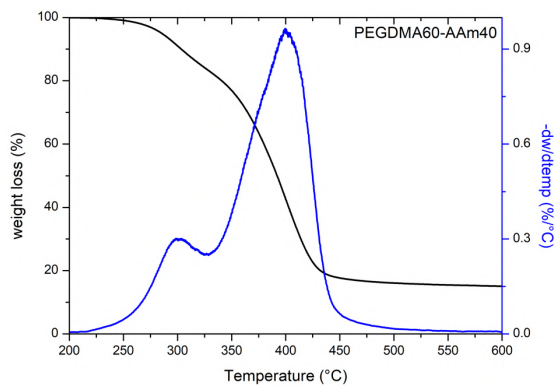
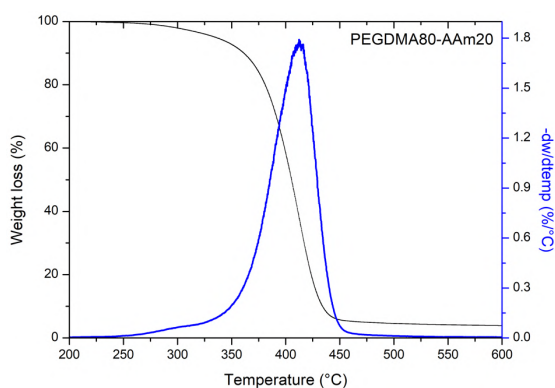
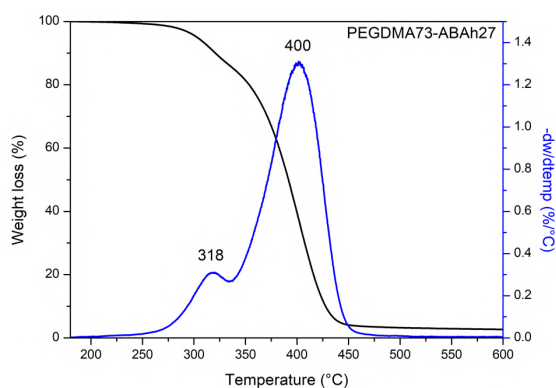
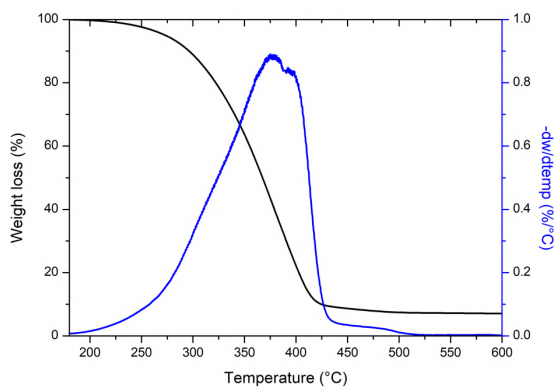
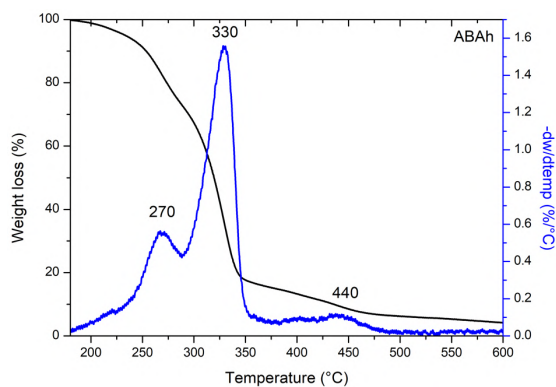
Table S1. PEGDMA-based CGs.^a

Sample	Monomer concentration (%)	Mean pore size (μm) ^b	Q_w water (%)	Porosity (%)	Yield (%)
PEGDMA-5%	5	84.0 ± 2.0	1950 ± 80	94.0 ± 2.0	90-93
PEGDMA-10%	10	40.0 ± 2.0	1600 ± 100	91.2 ± 0.4	89-95
PEGDMA-15%	15	32.0 ± 8.0	850 ± 90	85.0 ± 3.0	85-91
PEGDMA-20%	20	15.0 ± 6.0	600 ± 80	81.6 ± 0.9	86-90

^a Polymerization conditions: CQ and EDMAB: 2% w/w with respect to total of monomers. Polymerization time: 40 min; temperature: $-20\text{ }^\circ\text{C}$. Solvent: water.

^b Mean pore size was calculated from the distribution curves.

1.4 Thermogravimetric analysis of different CGs and dCGs



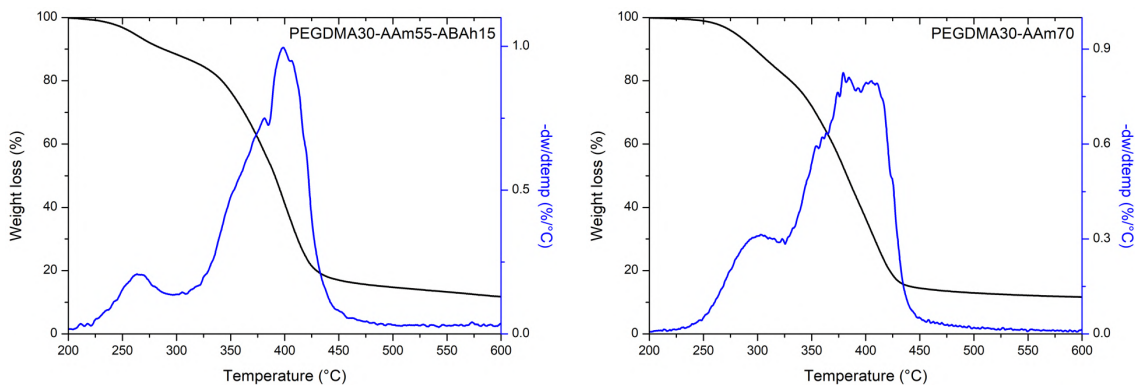


Fig. S6. TGA-DTA of different samples.

1.5 Morphology of CGs

To obtain the pore size distribution, SEM images were processed using ImageJ software. The general procedure was next: first, the scale, the bright and contrast was calibrated. Then, threshold was applied, considering the darkest areas as holes and pores. The “analyse particle” function was used to counting and measuring the pores. For convenience, mean Feret’s diameter was used, because of the non-spherical shape of the pore structure. Finally, pore diameter was used to provide the pore size and the pore size distribution, from different SEM images of each sample.

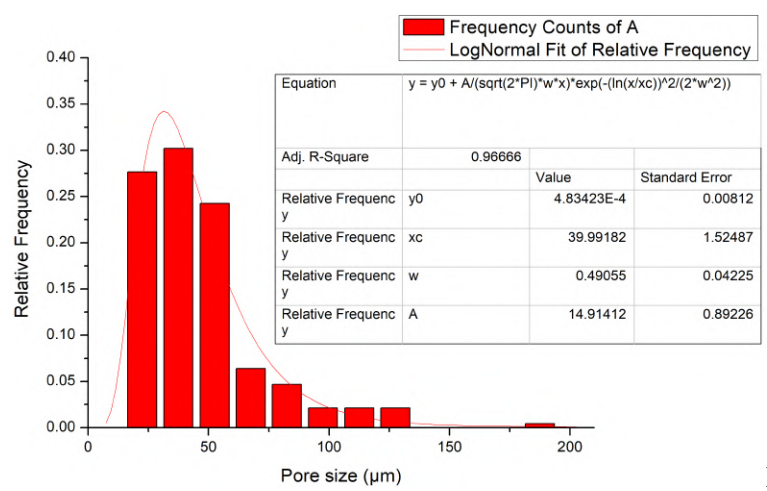
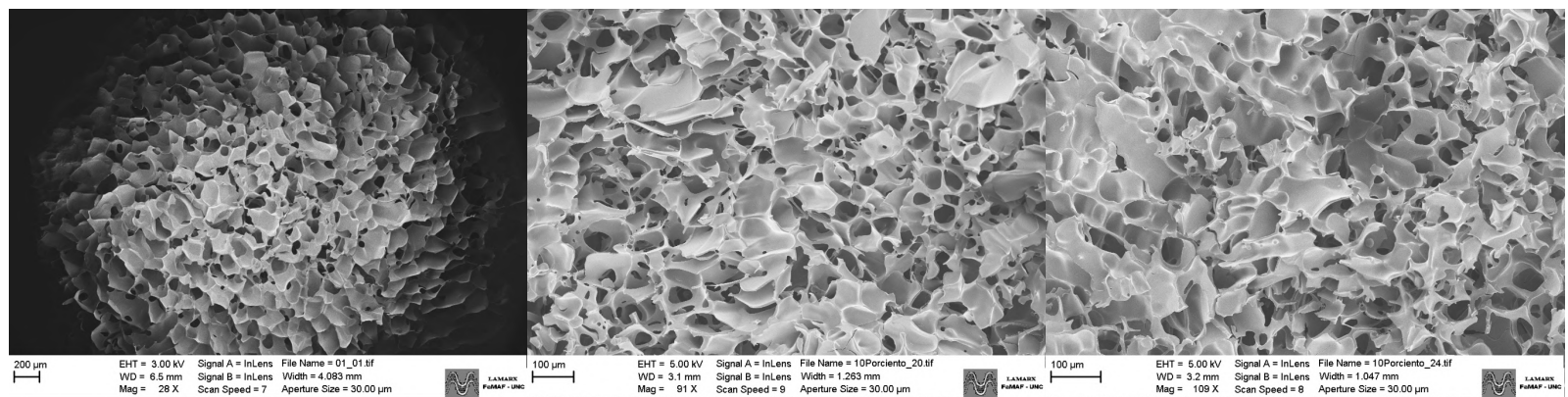


Fig. S7. SEM images and pore sizes distribution of PEGDMA100 cryogel.

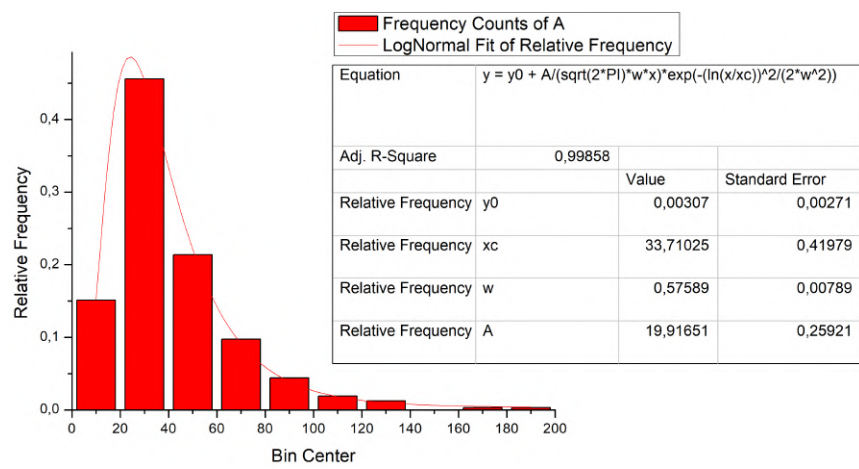
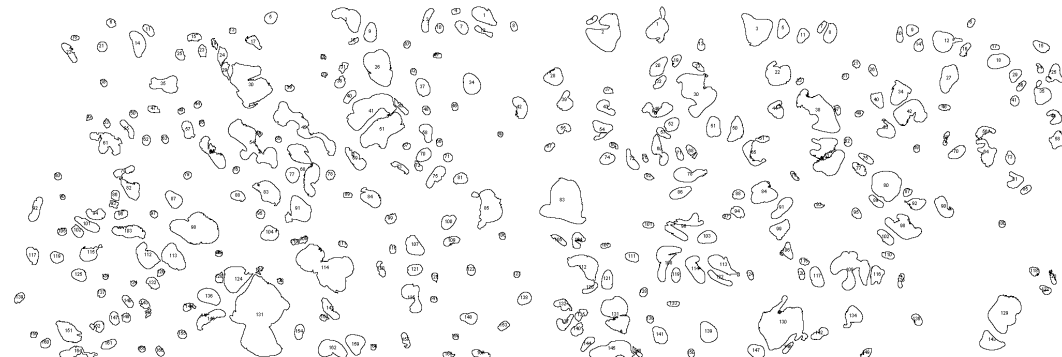
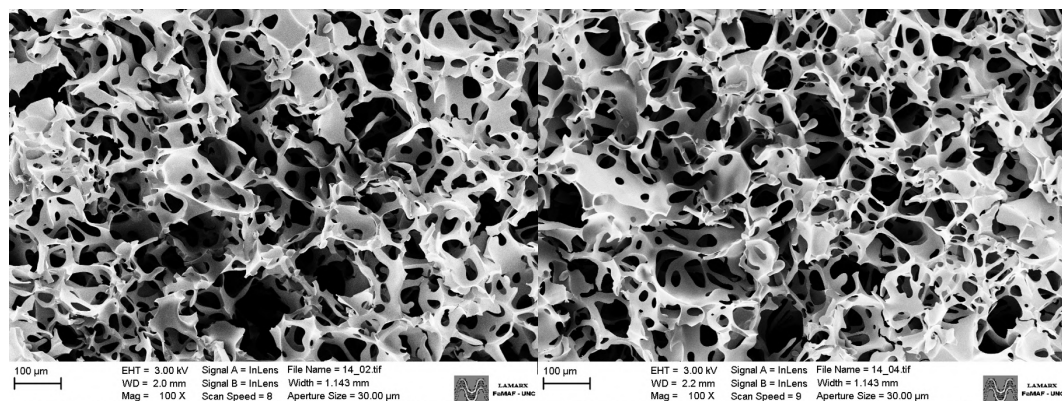


Fig. S8. SEM images and pore sizes distribution of PEGDMA80-AAm20

cryogel.

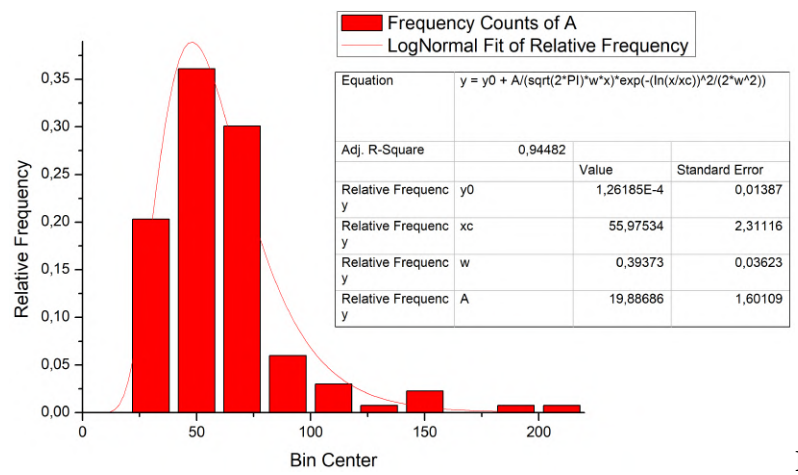
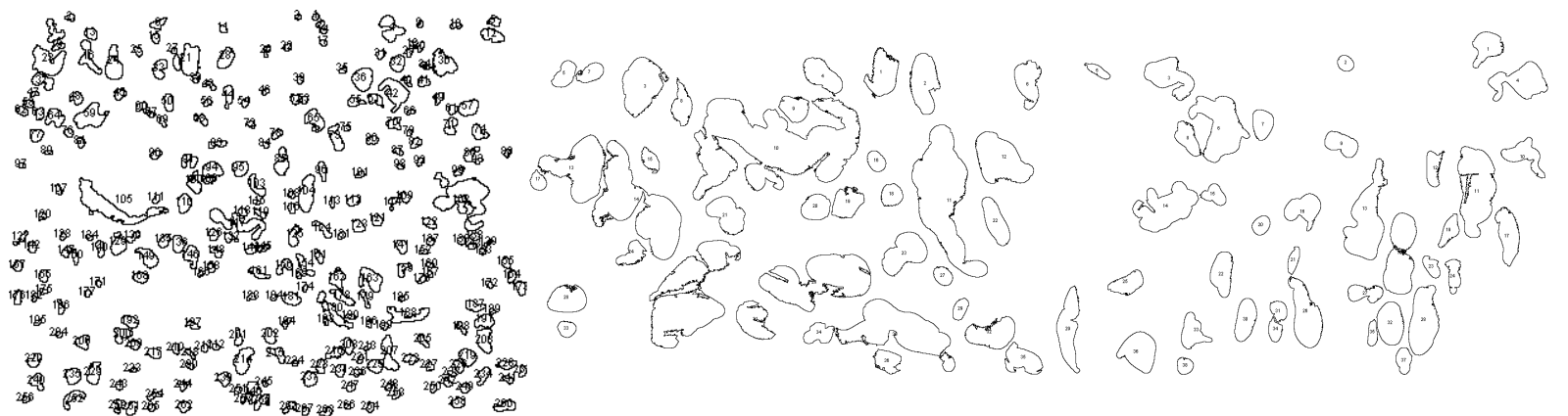
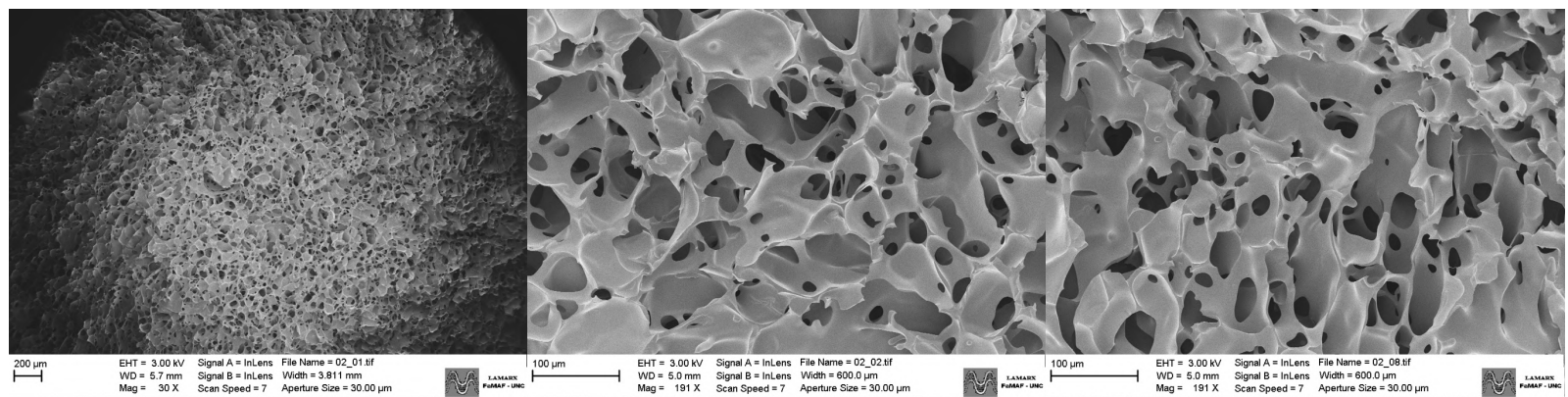


Fig. S9. SEM images and pore sizes distribution of PEGDMA60-AAm40 cryogel.

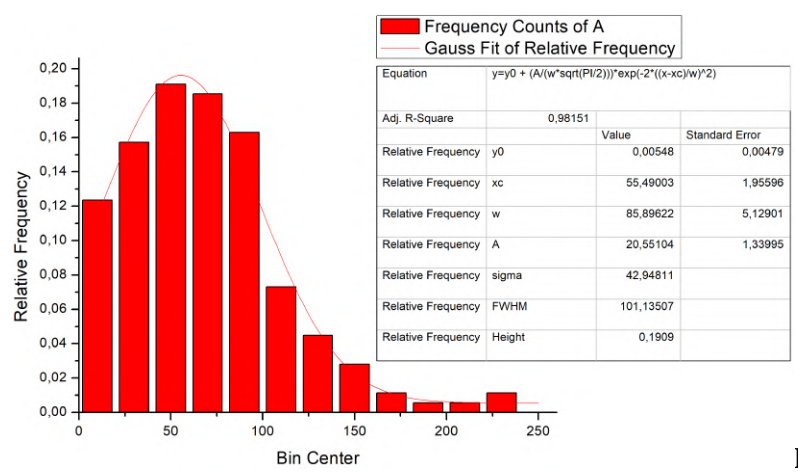
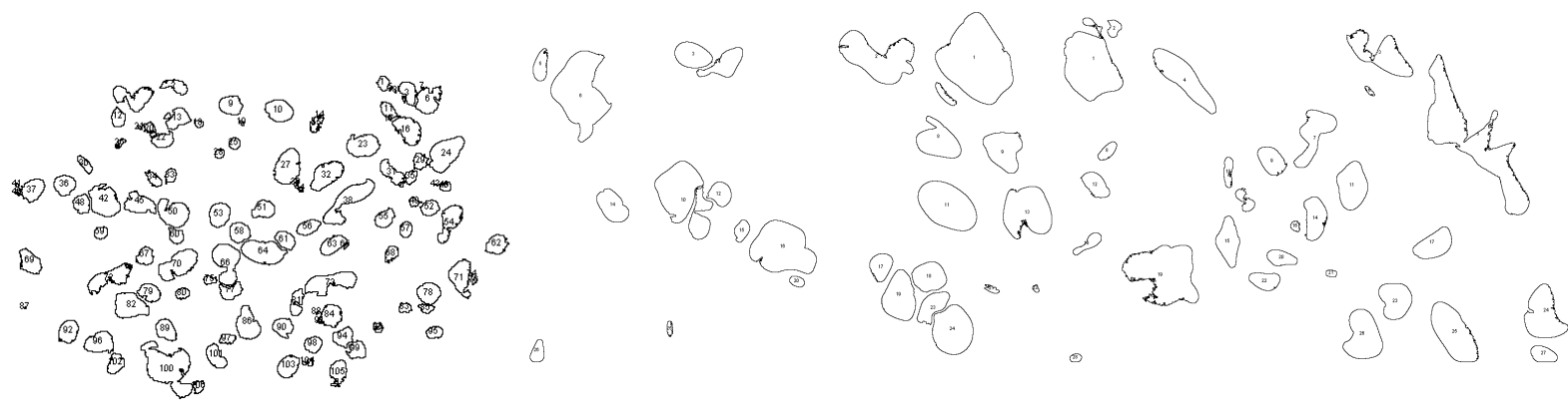
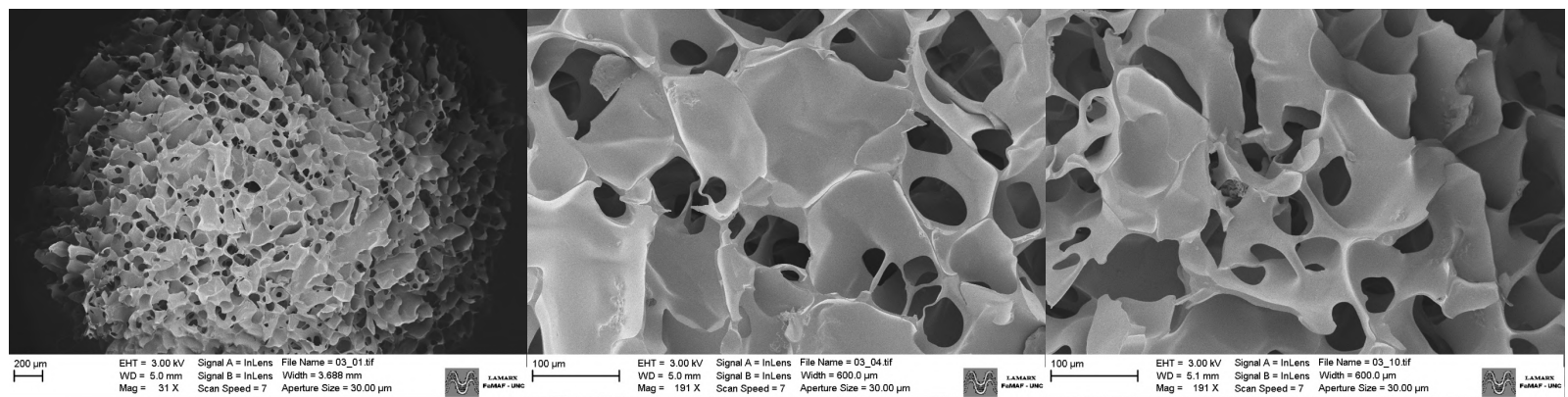


Fig. S10. SEM images and pore sizes distribution of PEGDMA40-AAm60 cryogel.

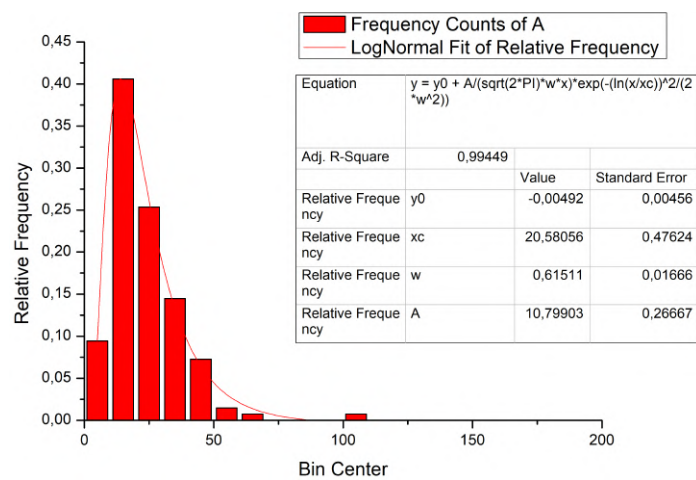
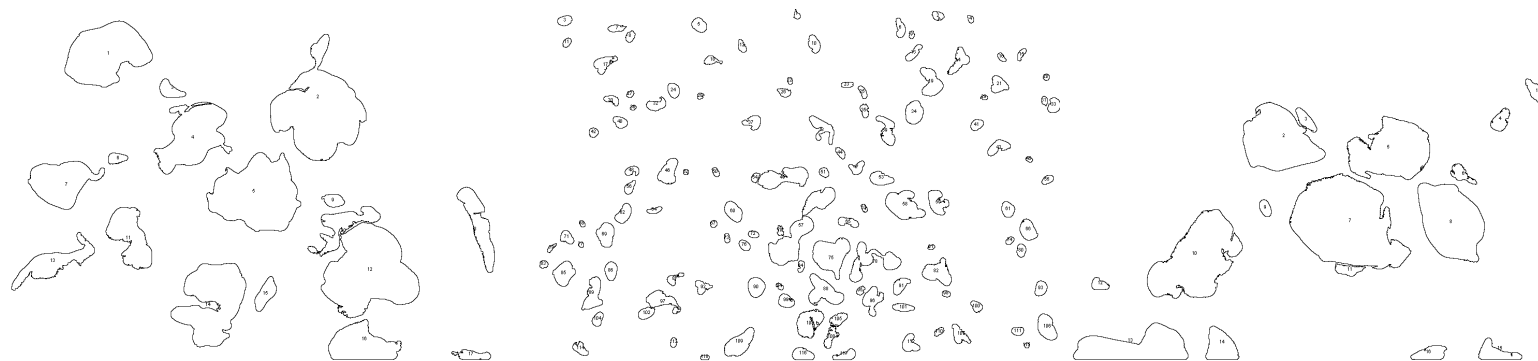
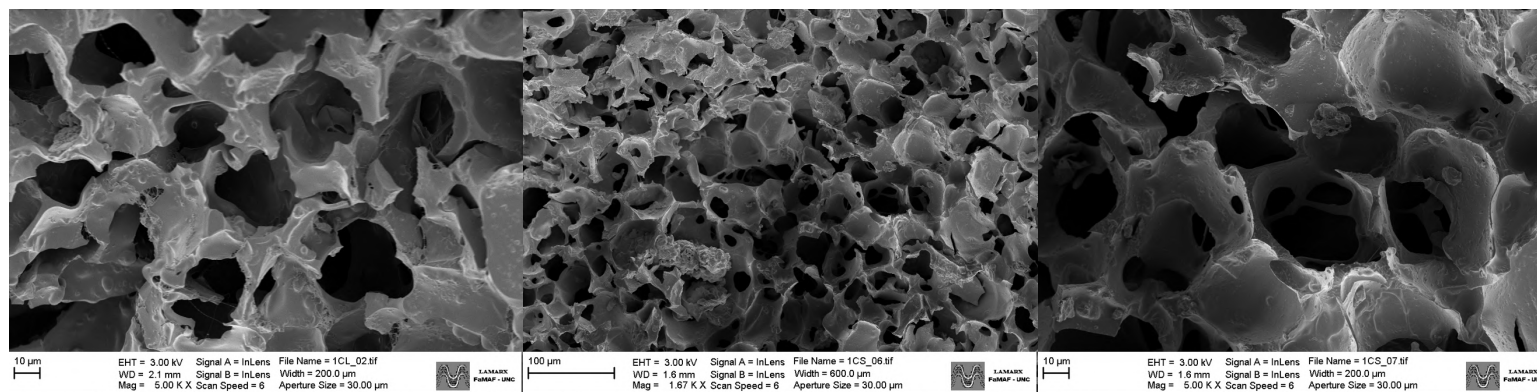


Fig. S11. SEM images and pore sizes distribution of PEGDMA30-AAm70 cryogel.

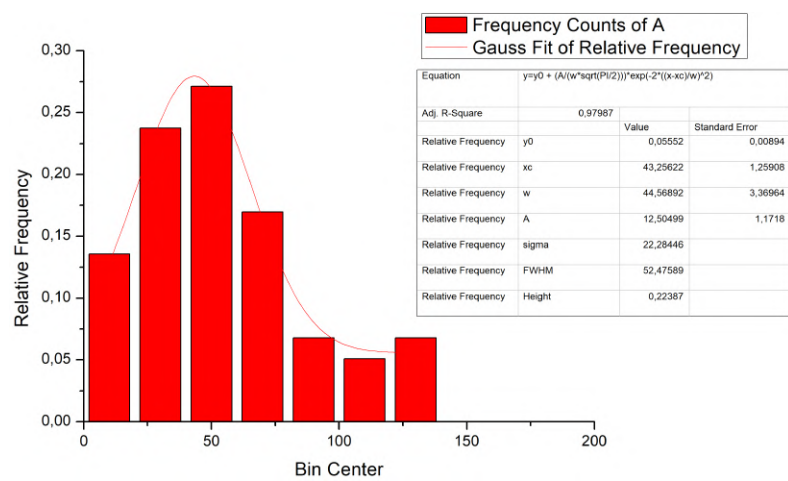
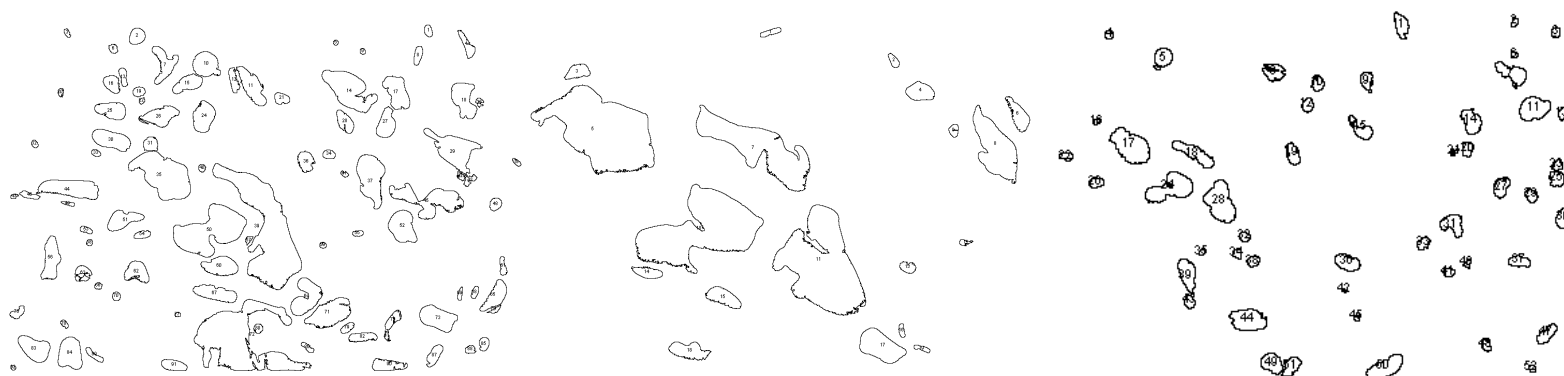
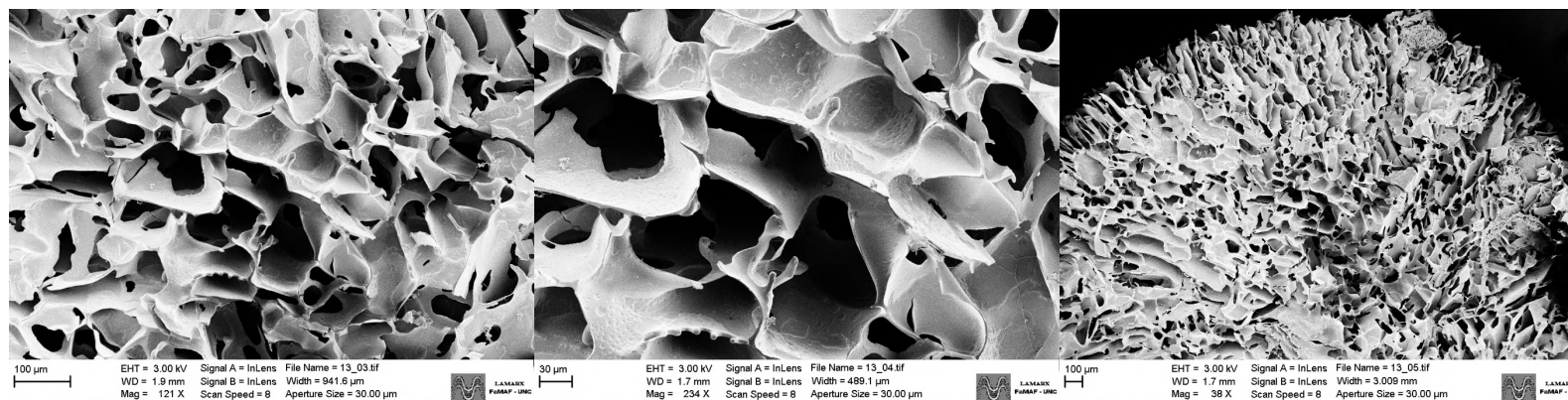


Fig. S12. SEM images and pore sizes distribution of PEGDMA80-AAc20 cryogel.

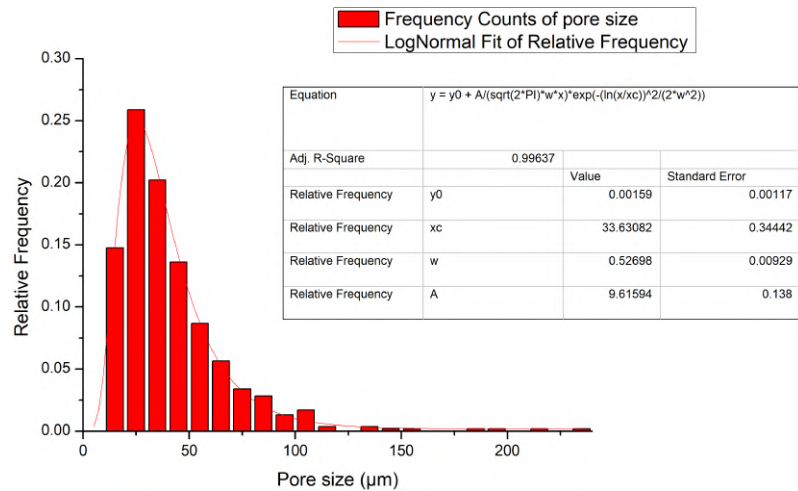
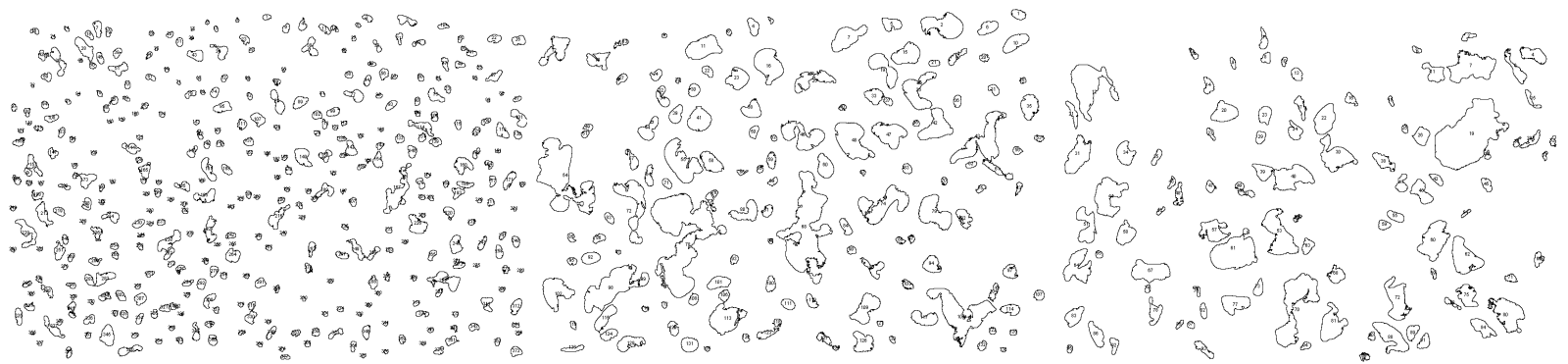
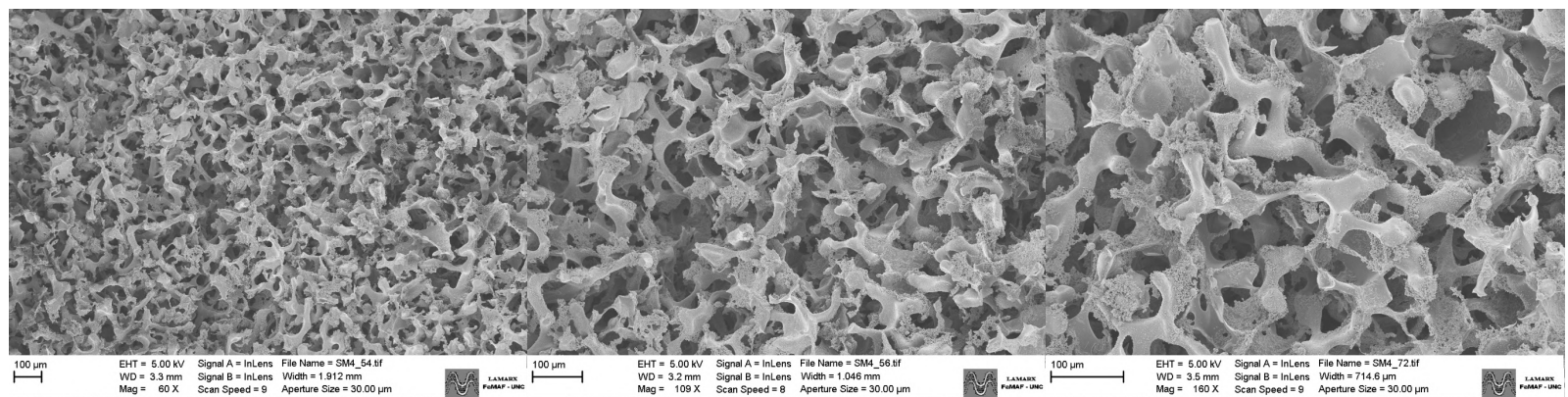


Fig. S13. SEM images and pore sizes distribution of PEGDMA60-AAc40 cryogel.

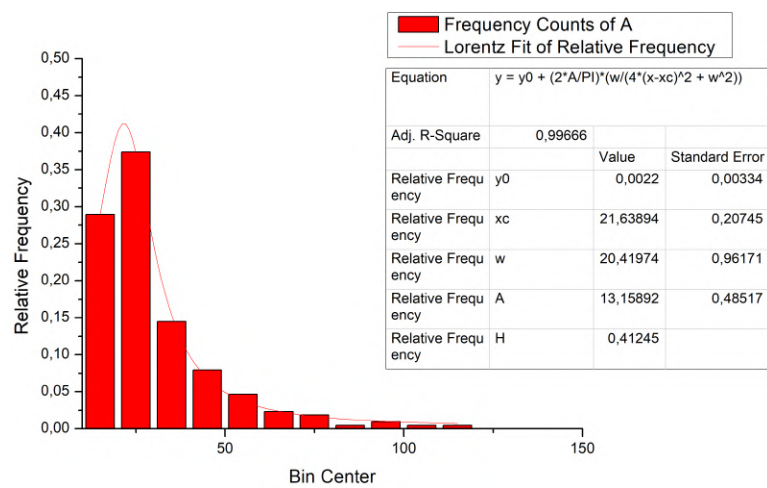
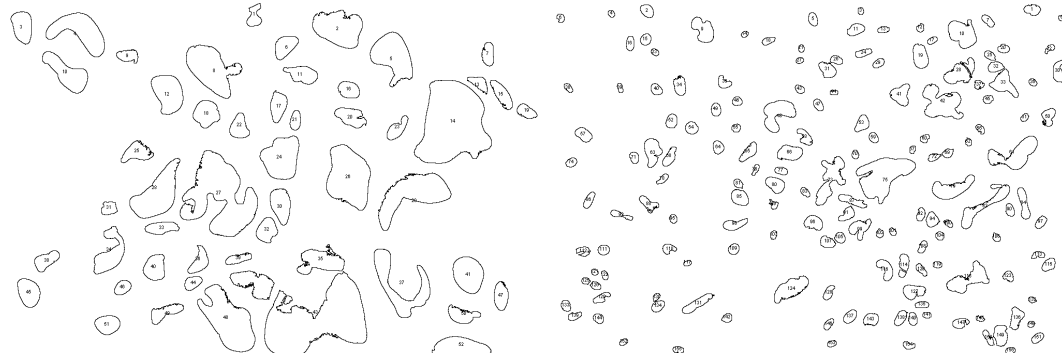
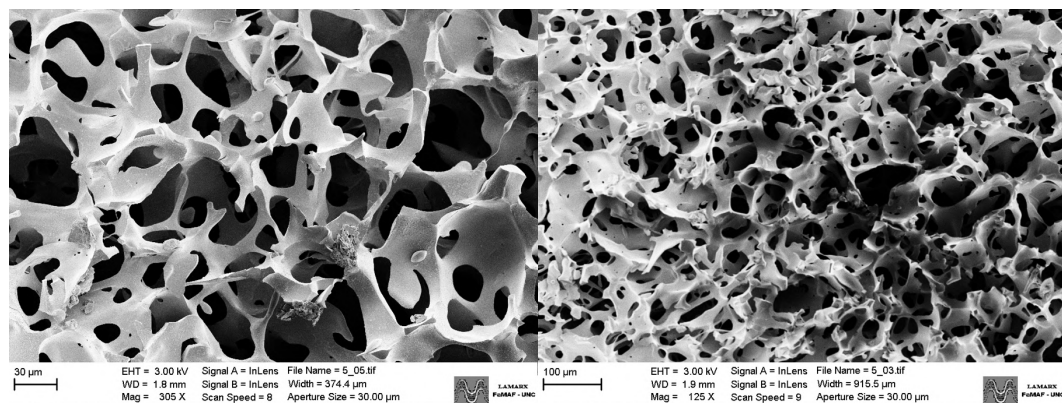


Fig. S14. SEM images and pore sizes distribution of PEGDMA40-AAc60 cryogel.

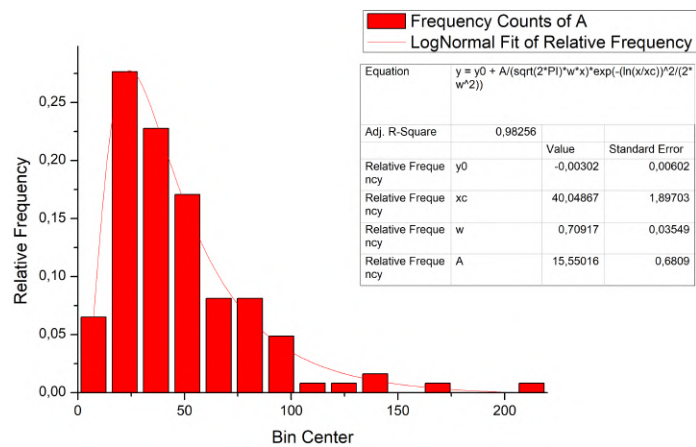
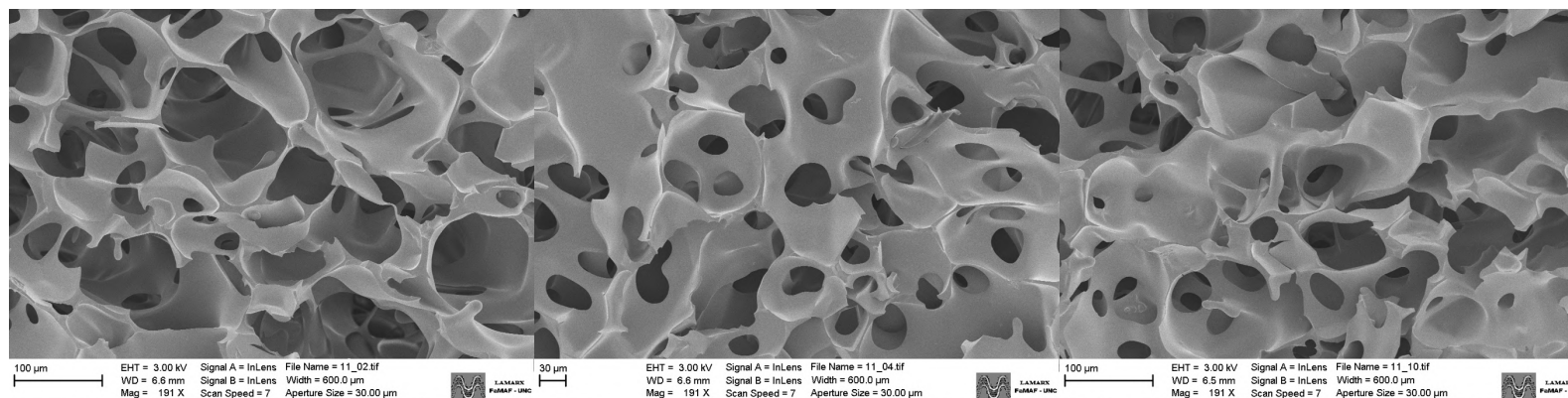


Fig. S15. SEM images and pore sizes distribution of PEGDMA30-AAm65-ABAh5 cryogel.

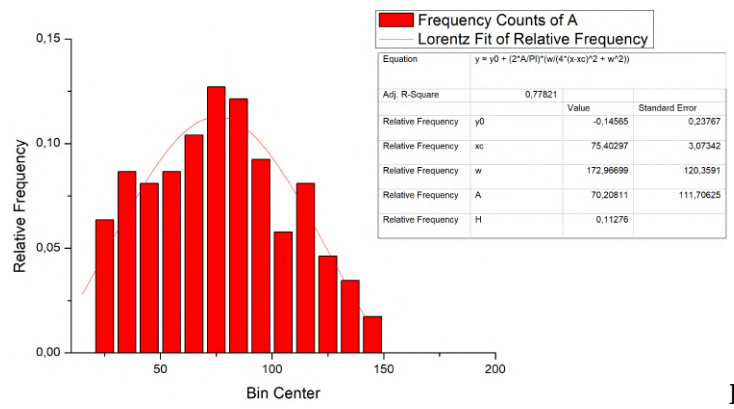
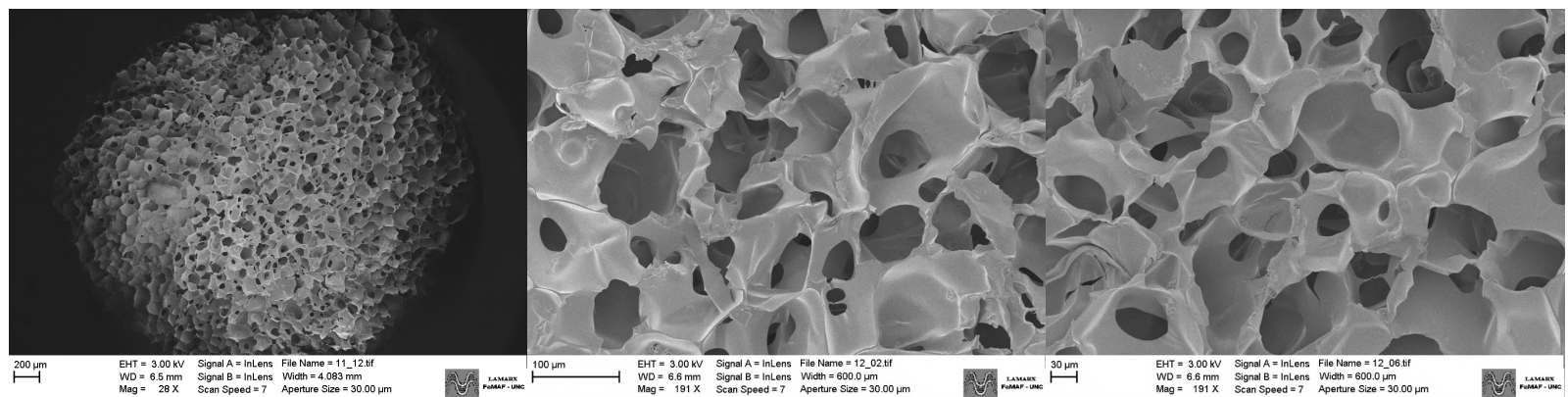


Fig. S16. SEM images and pore sizes distribution of PEGDMA30-AAm60-ABAh10

cryogel.

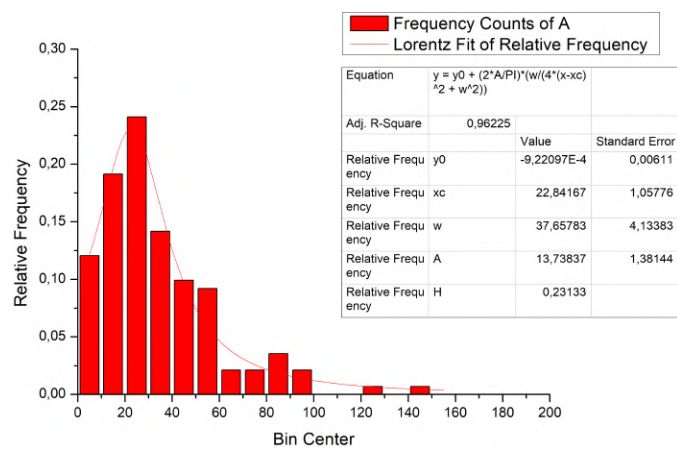
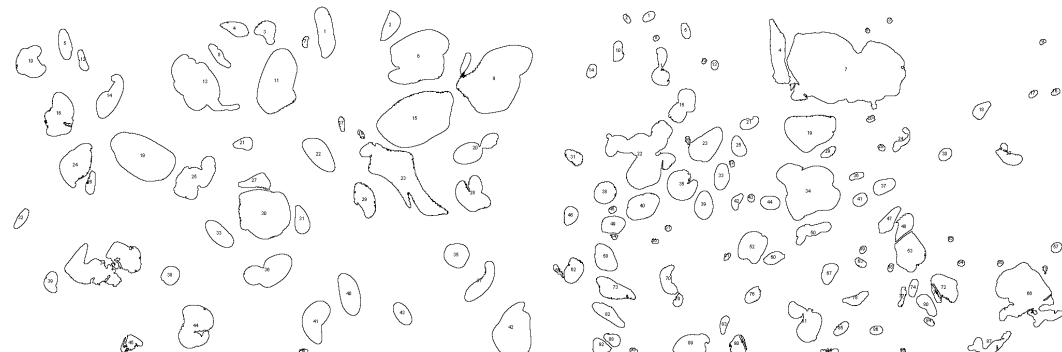
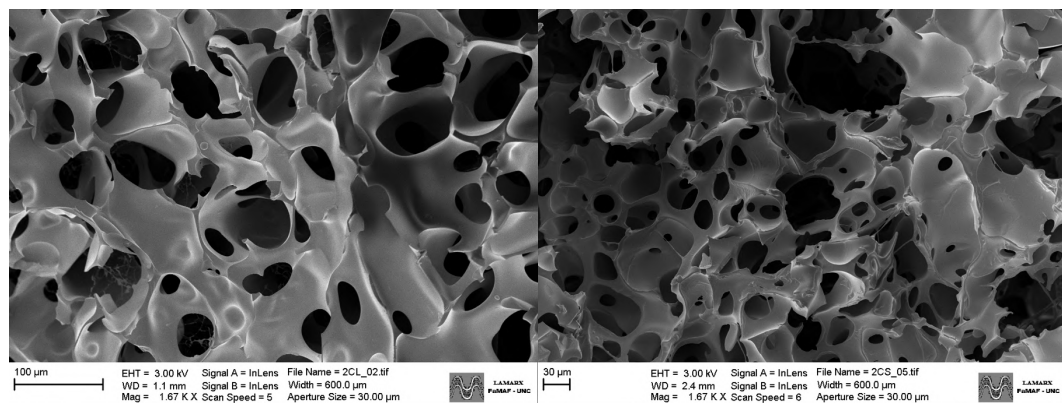


Fig. S17. SEM images and pore sizes distribution of PEGDMA30-AAm55-ABAh15 cryogel.

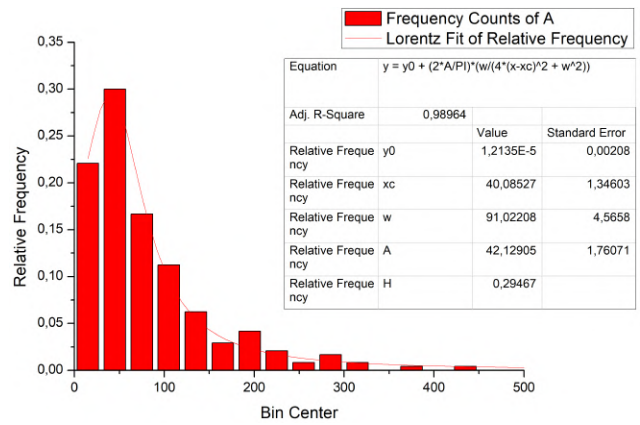
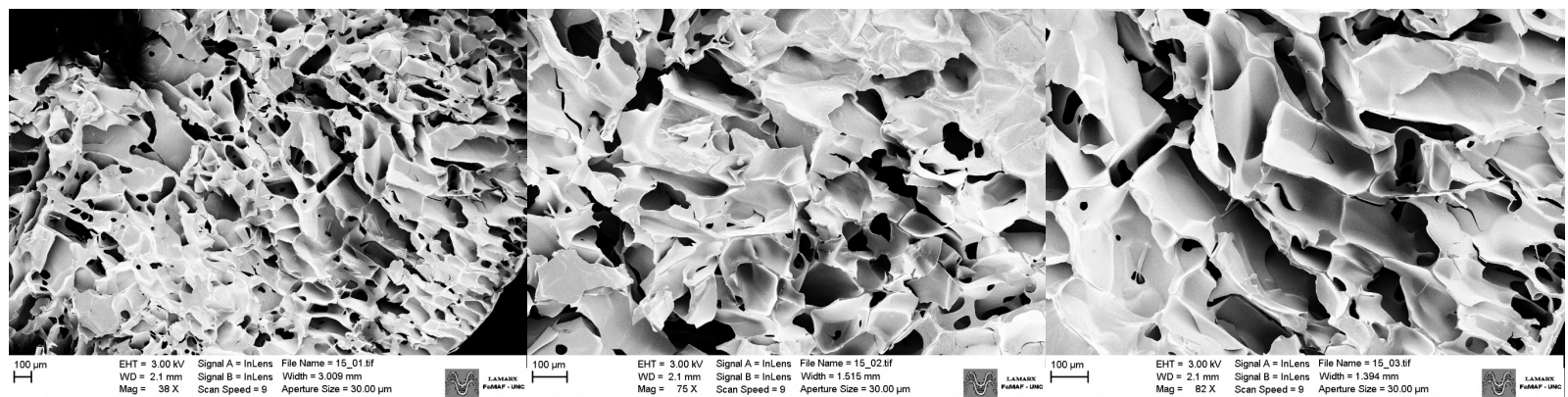


Fig. S18. SEM images and pore sizes distribution of PEGDMA73-ABAh27 cryogel.

1.6 CGs-Cu matrices

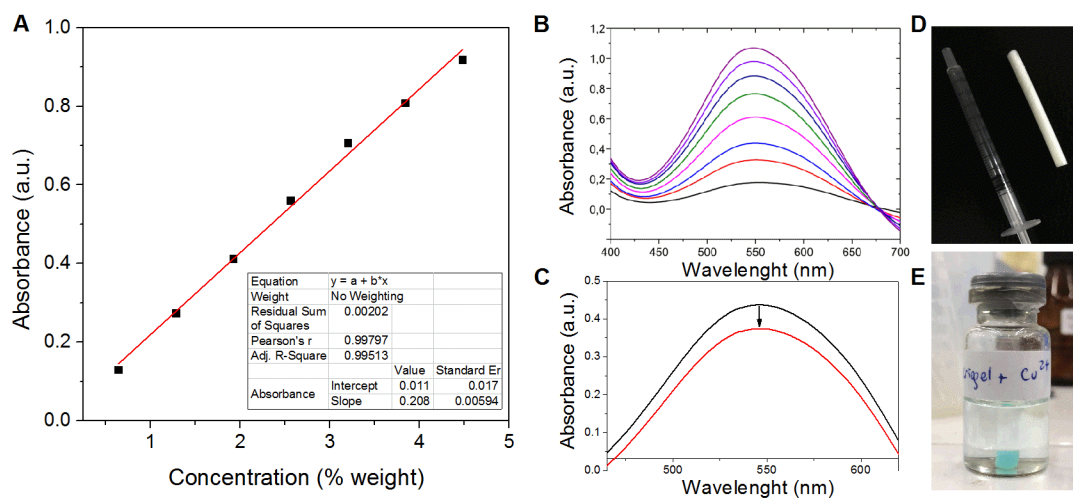


Fig. S19. **A), B)** Calibration curve of IgG in presence of EDTA/Cu complex. **C)** Difference between the UV-Vis absorption of IgG solution (control, black line) and IgG solution after contact with PEGDMA30-AAm55-ABAh15 (red line). **D)** Picture of synthetic cryogel and **E)** a cryogel sample under Cu^{2+} solution.